Large Area Freestanding Au Nanoporous Ultrathin Films Transfer Printed on Bendable Substrates and 3D Surfaces for Flexible Electronics

Issraa Shahine, Quentin Hatte, Maxime Harnois, Pierre-Yves Tessier

Large Area Free Standing Au Nanoporous Ultrathin Films Transfer Printed on Bendable Substrates and 3D Surfaces for Flexible Electronics

Issraa Shahine[1,2], Quentin Hatte[1], Maxime Harnois[3], Pierre-Yves Tessier[1]*

[1]Nantes Université, CNRS, Institut des Matériaux de Nantes Jean Rouxel, IMN, F-44000 Nantes, France.

[2]SATT Ouest Valorisation, Rennes, France.

[3]Institut d'Électronique et des Technologies du numéRique, IETR, Rennes, France.

*Corresponding author's email address: pierre-yves.tessier@cnrs-imn.fr

ABSTRACT

Conductive films based on metal nanomaterials are studied as electrical interconnects for flexible electronics. Among them, free standing ultrathin films are flexible, making them ideal candidates for integration onto 3D surfaces with complex shapes. Nevertheless, obtaining self-supported films of a few tens of nm with an area of several cm^2 without breaking them is difficult. The solution proposed in this work is to get the films floating on the water surface before transferring them to 3D flexible surfaces by a water transfer printing process. Herein,

we report the fabrication of stable and homogeneous Au nanoporous films with a thickness range of 6 to 60 nm and a floating surface area of several tens of cm^2 on the water surface. The process combines Au and Cu magnetron sputtering deposition, Cu dealloying and etching in acid vapor. We show that the transfer of such ultrathin films with a large area from the water surface onto the surface of flat flexible substrates or 3D surfaces is possible, maintaining conformability without significant electrical conductivity degradation. The thinnest films have a sheet resistance of about 10 Ω/□ with a transparency of about 50 % at 550 nm. Due to their specific nanostructuration consisting of nanopores and interconnected nanoligaments, these films transferred to flexible flat surfaces can withstand bending for at least 3000 cycles with a curvature radius of 1 mm. Moreover, we show that a transfer of a design to a complex curved surface of 3D objects is possible using a 6 nm layer whose role is to keep the geometry of the design during the transfer process.

Keywords: Gold, Copper, AuCu alloy, Dealloying, Etching, Nanoporous Thin Film, Free Standing Films, Flexible Electronics, Water Transfer Process.

INTRODUCTION

In many fields, smart objects require display and sensing functions integrated on their surface.[1–7] These objects are generally polymer materials of complex three-dimensional (3D) shapes and may be bendable or stretchable.[8,9] It is then necessary to have a conformability combined with the flexibility of the metallic circuit connections integrated on the 3D surface. This condition is one of the main concerns in the field of 3D flexible electronics based on thin films. The conservation of the stability and functionality of the integrated film on the surface is also a significant challenge. Biocompatibility and breathability in skintronics and wearable

bioelectronics applications.[10–12] and the transparency of the film in optoelectronics applications could also be required.[13–16]

The use of metallic thin films in the field of flexible and stretchable electronics is limited by the poor ability of the films to withstand high tensile stress and high bending cycles. The appearance of cracks in the metal film during bending cycles reduces or even disrupts its electrical conductivity[17,18]. Films based on metal nanowires[16,19–22], ultrathin nanoporous metal films[23,24] and films containing metal meshes or grids [12,25–27] have better abilities to withstand deformation thanks to their morphology adaptation without the appearance of cracks.[24]

On the other hand, more and more in the field of electronics, there is an increasing need to transfer electronic circuits onto surfaces of objects with complex 3D shapes. Among the many 3D transfer printing techniques, one convenient method is to realize the design of circuits in 2 dimensions (2D) using classical manufacturing processes in microelectronics and transfer these 2D architectures by water transfer printing methods onto 3D surfaces.[28–31] In these methods, the layers are a few hundred nm thick, placed on the top of a liquid surface and transferred to the 3D surface. The challenge lies in the risk of breaking the films under stress during the transfer from the liquid surface to the curved 3D surfaces of the object. The ability of a free-standing film to bend depends directly on the maximum strain ε it undergoes related to its thickness, t, and the radius of curvature, r, according to the following relationship:

$$\epsilon = \frac{t}{2r} \qquad \text{(equation 1)}$$

In this relation, r, is directly dependent on the local curvature of the surface on which the layer has to be transferred. Reducing film thickness reduces strain that appears during the transfer and thus limits the risk of break. The use of ultrathin film is therefore an exciting prospect, especially as these films can be nanostructured by bringing their morphology closer to the morphology of nanomesh to increase the flexibility or even the stretchability of the nanomaterial.

In this paper we study a new concept of metallic nanoporous film fabrication, consisting of simple fabrication steps to transfer such nanoporous films to 3D surfaces of complex shapes while keeping the good electrical conduction property of the metallic film. The process involves a chemical etching by a nitric acid of Cu sacrificial layer on which a pure Au or AuCu alloy ultrathin film is deposited. When AuCu instead of a pure Au film is used, a dealloying occurs during Cu etching step. Metal dealloying techniques to form nanoporous layers have been studied for a long time.[32–36] During the dealloying of AuCu alloy, the oxidized copper, present as solvated Cu^{2+} ions, is removed from the layer. Meanwhile, Au atoms are reorganized in the form of a nanoporous material that can have ligaments.[30] Another option is to use a pure Au layer deposited on Cu sacrificial layer. In this case, if the pure Au layer is thin enough, a reorganization into a nanoporous material happens during the Cu etching.[37,38] In this last case, the reorganization is due to the thermodynamic instability of such an ultra-thin layer.[39]

The oxidation of the metal to be removed, copper in this work, is usually done with acid solutions. However, this process is not suitable for very thin Au layers because it frequently leads to the delamination and fragmentation of the layer in the liquid.[30] The use of a nitric acid vapor instead of a nitric acid solution results in a dealloying and etching process of copper that avoids the film fragmentation.[30] In this paper, this process will be tested to produce a large-area, homogeneous nanoporous layer that is stable and easily transferable to the surface of liquid water, for subsequent easy transfer onto the surface of flexible and complex 3D-shaped substrates.

EXPERIMENTAL SECTION

Transfer printing concept

The fabrication process described in figure 1 includes Au and Cu film deposition step on a glass substrate by DC magnetron sputtering. The next step includes a nitric acid vapor treatment

to etch the copper sacrificial layer and to dealloy the AuCu based alloys. This etching/dealloying step leads to the formation of a thin nanoporous film that is easily detachable from the glass substrate and can be transferred onto the water surface.

The following step consists in peeling and transferring the ultrathin films to the surface of the water to end with a water transfer printing step onto the surface of the object to be coated. In this work, the ultrathin films were transferred onto 130 µm thick flexible polyethylene terephthalate (PET) polymer films for bending tests or onto 3D shaped surfaces of thermoformed PET sheets.

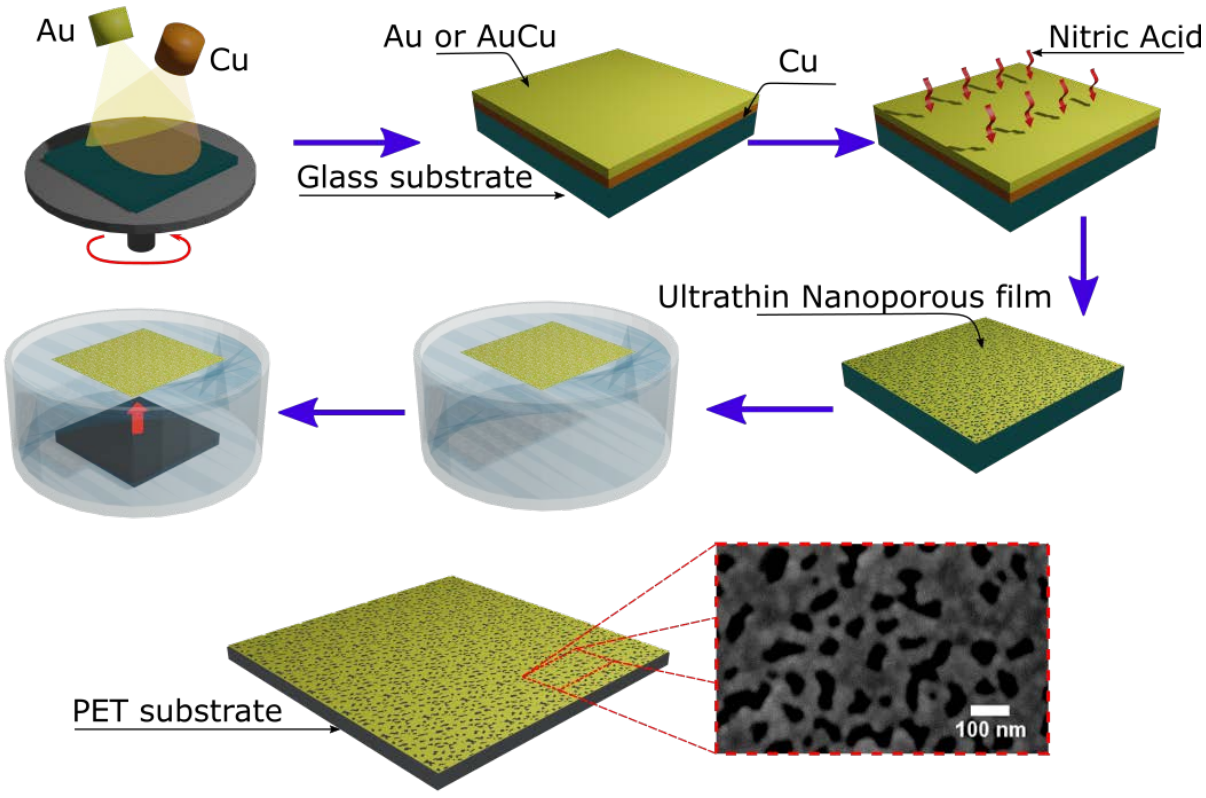

Figure 1. The protocol of the transfer process of Au membranes with the main steps: film deposition, acid vapor dealloying/etching, peeling and transfer onto the water surface, and water transfer printing to PET substrate to obtain Au nanomesh covering the substrate visible on the SEM image.

Film deposition

The gold charge loading deposited on the surface is a crucial parameter. It has been observed that for film thicknesses between 5 and 20 nm and an initial Au atomic concentration in the alloy between 11 and 23 at.%, cracks and isolated Au nanoporous microdomains appear on the surface after acid vapour dealloying.[30] In this study, the Au charge loading is increased by increasing the Au atomic concentration and by increasing the film thickness. The aim is to obtain a continuous Au nanoporous film without loss of electrical conductivity and a more robust and reliable transfer as a free-standing membrane floating on the water surface. Thin films are deposited by magnetron sputtering on a rotating flat glass substrate with an area of 10x10 cm^2. The first layer is a pure Cu film with a thickness of 10 nm. This film is used as the sacrificial layer. Then, Au or AuCu films are deposited on Cu sacrificial layer. The pure Au deposition rate deduced from profilometry measurement is 0.28 nm/s. The Au atomic flux deduced from weighing measurement is $1.7x10^{15}$ $cm^{-2}s^{-1}$. Two types of films are deposited: either a pure Au film by sputtering of Au target or $Au_{35}Cu_{65}$ alloy by co-sputtering of Au and Cu target. The composition of the alloy has been measured by energy dispersive X-ray spectroscopy (EDS) for thick films and this result is also consistent with the measured weight measurement of the respective atomic flux of Au and Cu atoms deposited on the substrate surface during co-sputtering. Details of the deposition are given in Supporting Information (SI: Film Deposition and EDS, Table S1).

The amount of Au deposited on the surface is controlled by the time of deposition. Three deposition times have been used to get 3 film thicknesses t corresponding to 3 surface densities of deposited Au atoms on the projected sample area, representing the area-normalized Au loadings (Table 1). For deposition of pure Au film, these times correspond to a deposited Au atomic density of 0.8 $x10^{17}$ cm^{-2}, 1.6 $x10^{17}$ cm^{-2} and 3.3 $x10^{17}$ cm^{-2}. For the deposition of $Au_{35}Cu_{65}$ alloy, the same deposition times are used corresponding to the same atom density of

Au on the surface. However, the film thickness is more important due to the incorporation of copper into the alloy. In the rest of the paper, since the layers are no longer homogeneous but become porous after etching and dealloying, we will use the equivalent Au film thickness to denominate the samples according to the 3 values of 13, 26 and 56 nm of pure Au films (Table 1). Additionally, an ultra-thin layer of 6 nm is also used as a support layer in the case of design transferred to 3D object surfaces (See the last part of this section). For comparison, the pure Au and AuCu films are also deposited directly on PET substrates and tested by bending tests.

Table 1. Designation of samples and main parameters of the films deposited on a 10 nm Cu sacrificial layer

Designation	Initial deposited film	Time deposition (s)	Film thickness (nm)	Deposited Au atomic density (x10^{17} cm^{-2})
6nm-Au	Pure Au	23	6	0.4
13nm-Au	Pure Au	47	13	0.8
13nm-AuCu	$Au_{35}Cu_{65}$	47	32	0.8
26nm-Au	Pure Au	94	26	1.6
26nm-AuCu	$Au_{35}Cu_{65}$	94	63	1.6
56nm-Au	Pure Au	201	56	3.3
56nm-AuCu	$Au_{35}Cu_{65}$	201	135	3.3

Etching and dealloying

Samples are submitted to a vapor of nitric acid to etch Cu sacrificial layer and to proceed to the Cu dealloying in the case of $Au_{35}Cu_{65}$ film. The use of an acid vapor instead of an acid solution is mandatory as it allows a softer treatment of the film avoiding fragmentation.[30] This

point is all the more important when the treatment is carried out on large areas of several tens of cm^2. To generate the vapor, the nitric acid solution (65%, 16 $mol.L^{-1}$) is placed in a closed container at a constant temperature of 298 K to maintain a constant vapor pressure in the closed chamber estimated at 380 Pa.[40] A layer of nitric acid solution then condenses on the sample surface leading to copper oxidation that produces solvated Cu^{2+} ions according to the following global chemical reaction:

$$Cu(s) + 4\ HNO_3(aq) \Rightarrow Cu(NO_3)_2(aq) + 2\ NO_2(g) + 2\ H_2O(aq)$$

The dealloying/etching time is set according to a visual control of the fading of the copper color from the sample over the glass to reach a uniformity of the apparent color of the acid vapor-treated sample. The dealloying/etching time is identified as 20, 40, and 80 minutes for the respective Au equivalent thicknesses 13, 26, and 56 nm alloys. Whereas, the etching of Cu sacrificial layer for samples with pure Au layers is 5, 7, and 9 minutes corresponding to an Au layer thicknesses of 13, 26, and 56 nm, respectively.

Transfer

The transfer process is performed as follows. The Au membrane is delaminated by the aid of the water supply in a suitable inclined water container. The film is left floating due to the surface tension forces on the distilled water surface for 5 min before the transfer to allow dissolving copper residue. Finally, the transfer onto flexible substrates is followed according to the water transfer printing technology developed to transfer film-based onto 3D object surfaces.[41–43] The PET substrate to be coated is put in water under the floating Au film (Figure 1), and the water level is lowered so that the film can be deposited on the PET surface.

Characterization techniques

Scanning electron microscopy (SEM) imaging is carried out on a JEOL JSM 7600 F microscope at 5 kV. The chemical composition of the alloy is measured by EDS on films with a thickness in the range of 500 nm – 1 µm (See SI - Film Deposition and EDS, Table S1). EDS is performed by a JEOL 5600 microscope operating at 15 kV. X-ray Photoemission Spectroscopy (XPS) measurements are carried out on an AXIS Nova from Kratos using a monochromatic Al Kα X-ray source (1486.6 eV). The spectra are recorded with a pass energy of 20 eV. The optical transmittance of the dealloyed/etched films finally transferred onto PET substrates is measured using a Perkin lambda 1050 equipped with a 150 mm integrating sphere. The sheet resistance is measured by using a digital multimeter (Keithley 2401) with a four-point probe setup. Bending tests are carried out on a homemade curvature bench.[30]

RESULTS AND DISCUSSION

The uniform change of color of the samples after the dealloying/etching is the result of the copper oxidation. Previous XPS analyses of the dried dealloyed surface have confirmed the presence of copper residue as copper nitrates and copper oxide[30]. The copper residue deduced from XPS represents less than 3 at.% of the total atomic concentration on surface after rinsing, transfer onto PET and drying of the sample (See SI: XPS). It corresponds to a ratio of Au atomic concentration over Cu atomic concentration equal to about 5.2 to be compared to the initial ratio of $Au_{35}Cu_{65}$ alloy before dealloying equal to 0.54.

When the Au thickness is lower than 13 nm, the electrical conductivity of the film cannot be maintained due to the presence of cracks resulting from exposure to acid vapors (Figure 2a). Thus it is not possible to obtain a transfer of the membrane onto the surface of the PET substrate without loss of electrical conductivity unless to percolate the separated Au islands floating on the water.[30] However, equivalent thicknesses of 13 nm and above show a homogeneous surface after etching of Cu layer in acid vapor (Figure 2b). In this condition, a robust and easy transfer

onto the surface of the water without any cracks is obtained, and then the water transfer printing step on the flexible substrate is carried out without the need for the delicate percolating step.

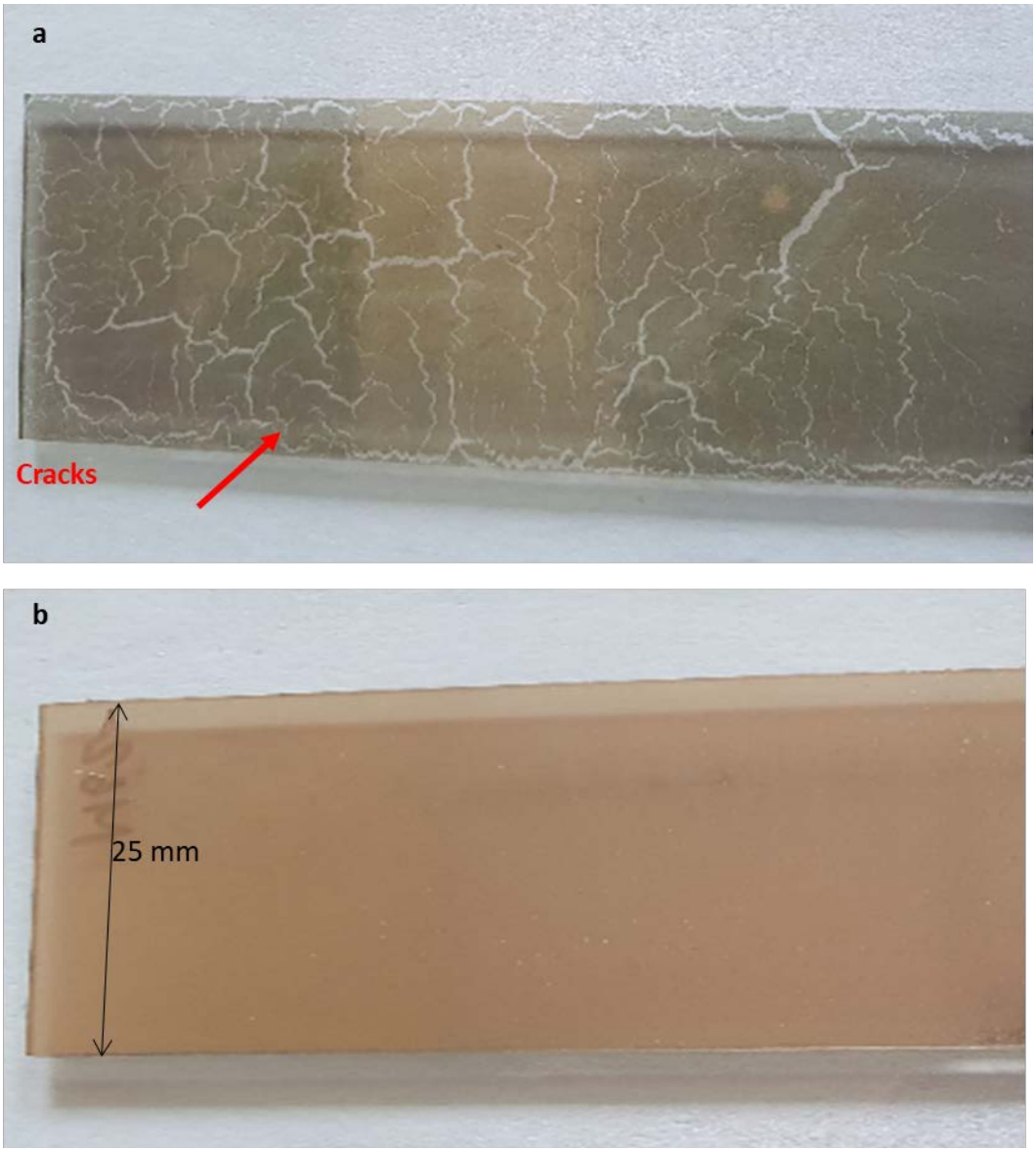

Figure 2. Optical picture of sample deposited on a glass microscope slide after Cu etching in nitric acid vapor (a) 6 nm Au thickness, (b) 13 nm Au thickness.

After the dealloying/etching and the water transfer printing onto the PET surface, the surface nanostructuration of the film is visible on SEM images (Figure 3). For the thinnest Au equivalent thickness of 13 nm, nanopores and connected nanoligaments on the surface of the 2

types of samples are observed. The size of the pores and the width of the ligaments are higher in the case of the transferred pure Au films. For thicker films of 56 nm, this type of nanostructuration is also visible in the case of transferred dealloyed AuCu layers but does not occur when pure Au layers are transferred.

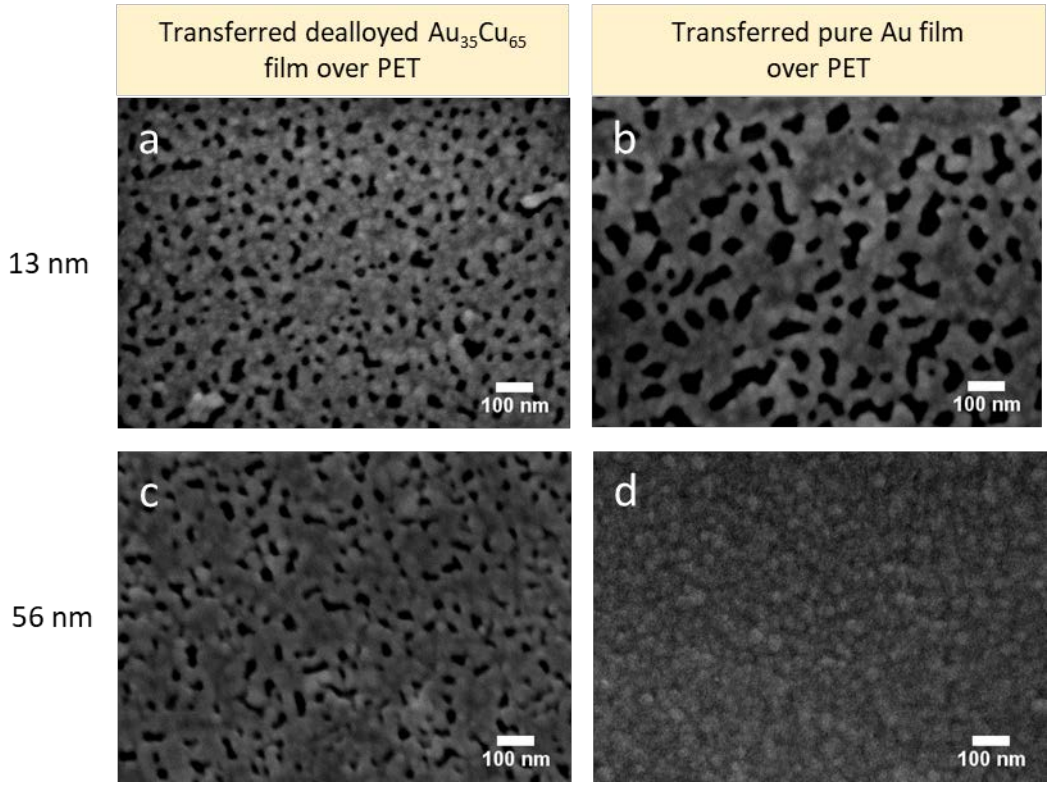

Figure 3. SEM images of the 13nm-AuCu (a), 13nm-Au (b), 56nm-AuCu (c) and 56nm-Au (d) films after dealloying/etching and transfer onto PET surface..

For the dealloyed films, the observed porosity is attributed to the removal of copper atoms from the alloy combined with the Au surface diffusion process during the dealloying resulting in the formation of a planar gold skeleton consisting of nanopores and interconnected nanoligaments.[30] For the transferred pure Au films, the formation of pores and ligaments for the 13nm-Au transferred sample is attributed to the reorganization of the very thin Au layer during the etching of Cu sacrificial layer as it has already been observed in previous works[37,38].

Indeed, below a few tens of nm in thickness, the thermodynamic instability leads to a reorganization of their nanostructure.[39] On the other hand, thicker films are thermodynamically more stable. It is the reason why we assume that nanopores and nanoligaments are not observed for the 56nm-Au transferred film on the SEM image in Figure 3.

The evolution of the optical transmittance T as a function of the sheet resistance $R_{\square}$ is given in Figure 4. Measurements are carried out on transferred layers to flat PET films with an area of 10x10 cm^2 (SI – Optical transmittance – Figure S2).

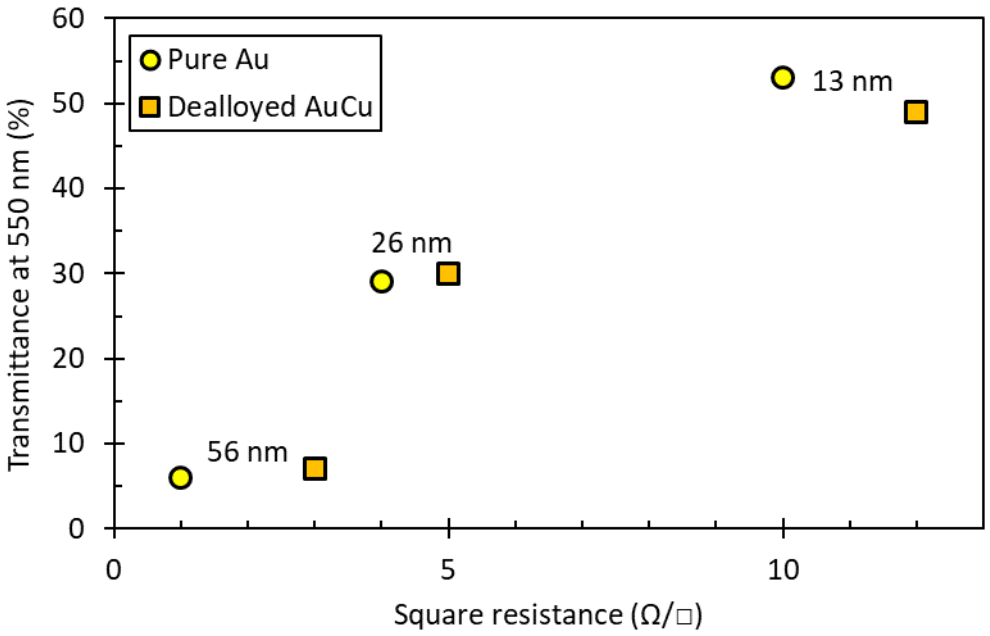

Figure 4. Optical transmittance of different Au equivalent thicknesses at wavelength λ=550 nm as a function of the sheet resistance for pure Au and dealloyed AuCu transferred layers to PET film.

We observe the typical trend characterized by an increase of T with $R_{\square}$. The trends are almost identical for both types of film. We move from films with low sheet resistance of few Ω/□ but

practically not transparent to film of about 10 Ω/□ and semitransparent. However, we can notice that the sheet resistance of pure Au transferred films is lower than that of dealloyed AuCu transferred films for the same Au equivalent thickness. This higher resistance measured for dealloyed films could be attributed to the microstructural defects and specific morphology induced by the dealloying process. Residual copper at very low concentration inside the Au ligaments may also play a role. Indeed, the role of the remaining less noble element in tuning the Au microstructure and in modifying the catalytic and electrochemical properties has been demonstrated.[44]

Flexion tests are performed on all the samples to investigate the evolution of the resistance as a function of the number of cycles to bend the samples on PET films. For the bending test, Au nanostructured metal strips a 3 mm wide and about 80 mm long are transferred onto PET film. To evaluate the behavior of the samples under bending tests, first for each sample we have extended the number of cycles with a curvature radius, r, of 10 mm to 1000 cycles followed by 1000 cycles with r set at 5 mm, then followed by 1000 cycles with r at 1 mm. The transferred layer is on the convex PET surface during the bending to be subjected to tensile stress. The resistance for each sample measured at its initial flat state, R_0, is chosen as the reference and at each cycle, the flat resistance, $R_{Flat,}$ and the curved resistance, $R_{Curved,}$ are measured. We define the relative variation, %R, by the relation:

$$\%R = \frac{(R_{curved} - R_0)}{R_0} \times 100 \qquad \text{(equation 2)}$$

The evolution of %R is shown in Figure 5. Overall, whatever a given Au equivalent thickness, the behavior is qualitatively the same. The pure transferred layers have the smallest increase in resistance after 3000 cycles and even we can observe a slight decrease as a function of the number of cycles up to 2000 cycles. After 2000 cycles, when a curvature radius of 1 mm is applied, we observe a slight increase of few percent except for the 26nm-Au sample for which a stable decrease is measured until 3000 cycles. In contrast to the transferred pure Au films, the

behavior of the transferred dealloyed films differs significantly. These films exhibit a continuous increase in resistance with the number of cycles and a strong increase as soon as the radius of curvature goes from 5 mm to 1 mm after 2000 cycles. However, the resistance evolution for these films remains relatively stable up to 3000 cycles. It is worth noticing that the final increase of the resistance remains limited even after 3000 cycles. In conclusion, both the transferred dealloyed films and the transferred Au pure layers, whatever their equivalent Au thickness, can remain conductive under these very hard conditions of test. They exhibit a relative stable increase in resistance even after 3000 cycles at 1 mm curvature radius. Nevertheless, for a given Au thickness, the lowest increase in resistance always corresponds to the pure transferred Au layers.

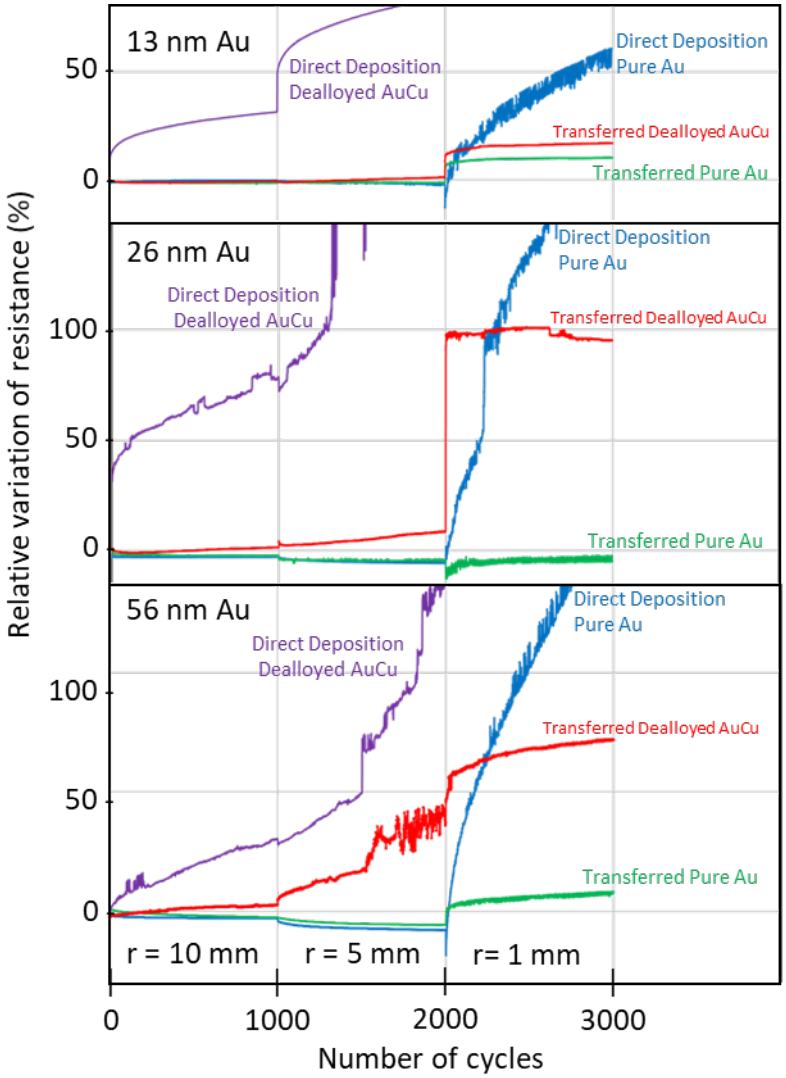

Figure 5. Evolution of the relative variation %R of the transferred films to PET as a function of the number of bending cycles for Au equivalent thickness 13 nm, 26 nm, and 56 nm. The first 1000 bending cycles correspond to a curvature radius of 10 mm, followed by 1000 cycles with a curvature radius of 5 mm, and finally 1000 cycles with a curvature radius of 1 mm. For comparison, the behavior of films deposited directly over PET is shown.

For comparison, we can see in figure 5 the evolution of pure Au films directly deposited over PET. These films follow the same behavior as the transferred pure Au films until 2000 cycles but as soon as a 1 mm curvature radius is applied, a continuous increase of their resistance is observed without any stabilization until 3000 cycles. As with the direct deposition of pure Au

films, the direct deposition of AuCu films on PET followed by dealloying shows a continuous increase in resistance with the number of bending cycles. This increase is evident from the very first cycles, irrespective of the equivalent Au thickness.

In summary, the sequential steps of etching/dealloying, film transfer onto the water surface and water transfer printing limit the decrease of the electrical conductivity for films subjected to tensile cycling. Films deposited directly on PET cannot withstand the tensile strain induced by cycles with a curvature radius of 1 mm and a continuous degradation of their performances is observed with cycles. It is known that the direct Au deposition on glass or PET follows a Volmer-Weber growth due to the low surface energy of the substrate. It means that the formation of a continuous Au film on the surface follows a coalescence mechanism of the Au grains to get a final typical columnar morphology for thick films. In the case of a direct deposition subjected to tensile strain, the surface connecting Au columns contains porosity and defects that are at the origin of the degradation of the resistance under strain. In the case of transferred films, we assume that the process of etching of Cu sacrificial layer leads to a reorganization of the Au film morphology at the interface, which enables a continuous connection by the Au ligaments. Therefore, we attribute the excellent flexibility performance of the transferred films to this 2D specific morphology induced by the Cu etching process. Although the behavior of the transferred dealloyed samples is not as good as that of the transferred pure Au samples, we assume that it is also this specific 2D morphology that enables them to achieve stabilization of their electrical resistance even after enduring 3000 cycles. The reason why the performance of these dealloyed samples is not as good as that of the pure samples is not fully understood. We can notice that the typical size of pores and ligaments differs between dealloyed and pure samples, even for the same equivalent Au thickness (see Figure 3). This difference in morphology can play a role. Moreover, the dealloying mechanism of a AuCu solid solution implies a strong phase transformation from the solid alloy solution to

the pure Au phase[34]. Microstructural defects and complex strain state[45] can appear during this transformation. These effects could also be a reason for the high observed resistance and low flexibility of the transferred dealloyed films compared to the pure Au transferred films.

If we focus on the behavior of the films during bending cycles with a radius of curvature of 1 mm, we observe a stable variation of the resistance between the flat and the curved position of the film as a function of the number of cycles (Figure 6). The relative variation of resistance between flat position R_{Flat} and curved position R_{Curved} remains lower than 7 %.

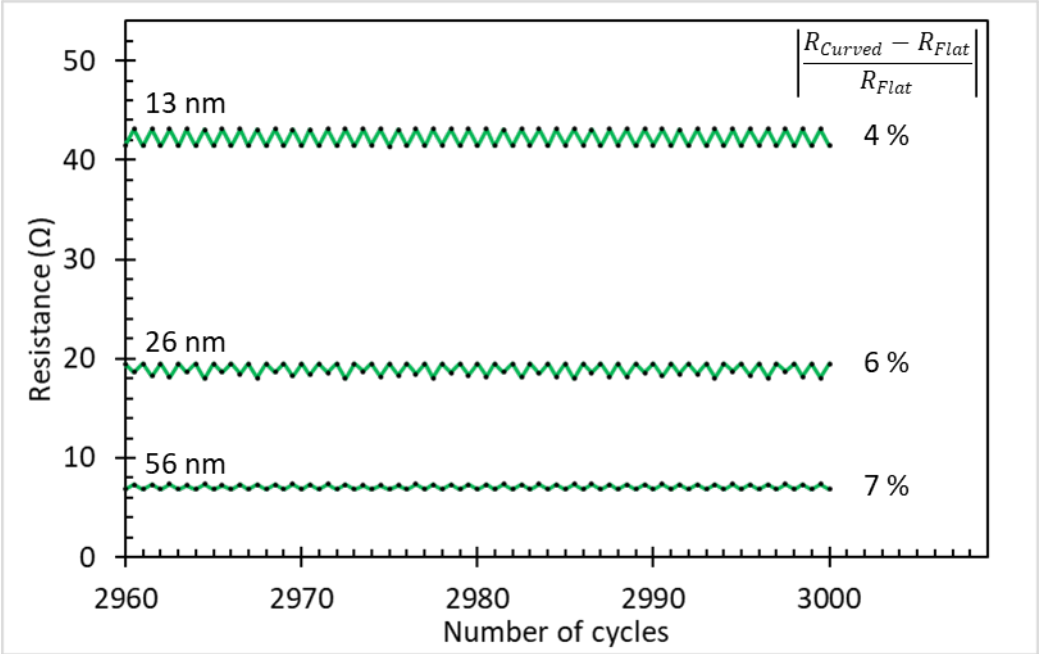

Figure 6. Evolution of the resistance of the transferred pure Au films to PET from flat position to curved position (Radius = 1 mm, ε = 6.5 %) and as a function of the number of bending cycles after 2950 cycles. The relative variation of resistance between flat position R_{Flat} and curved position is given in the figure for each thickness.

The 26nm-Au sample represents the best condition in the context of electrical connections for flexible electronics applications where the aim is to maintain constant resistance under

strain. Indeed, for this sample, we observe a very low variation of the resistance compared to the initial resistance along the 3000 cycles of the flexible test even with a 1 mm curvature radius (Figure 5) and the variation of resistance between curved position and flat position observed after 3000 cycles remains small (Figure 6) and can be considered negligible to first order. This is why this condition is chosen to test the water transfer of a pattern onto a PET 3D surface.

For the transfer of a pattern onto a 3D shaped surfaces of thermoformed PET sheets (See SI: 3D surface design), the layers are deposited using hard masks consisting of horseshoe lines (See SI: Horseshoe design). Beforehand, to maintain the pattern on the water surface during the transfer, a 6 nm thick layer of gold is deposited as support (Figure 7). This step is mandatory. Transfer without this support layer has been tested, but in this case it is impossible to prevent the distortion of the pattern when the Au layer is transferred onto the water surface after etching Cu sacrificial layer. It is not possible to use a polymer film easily removed as a support layer for design transfer, because for complex 3D surfaces with positive Gaussian curvature (e.g. spherical surface) or negative Gaussian curvature (e.g. saddle surface), the polymer film will form wrinkles and folds that will prevent conformal 3D surface coverage. With a 6 nm thick Au support layer, horseshoe lines can be transferred to the 3D surface with excellent conformability (Figure 8). The lines remain homogeneous without almost any cracks whereas a lot of cracks appear on the surface of the 6 nm support layer. Although this layer cracked, it nevertheless maintained the horseshoe pattern during the transfer from the water surface to the object to be covered. As shown in the SEM image (See SI – SEM image), the 26 nm thick line deposited on the 6 nm thick support layer is nanoporous after Cu etching and transfer. The value of the sheet resistance of the line is 6 Ω/□ and is well consistent with the value measured for layers transferred to a flat surface (Figure 4).

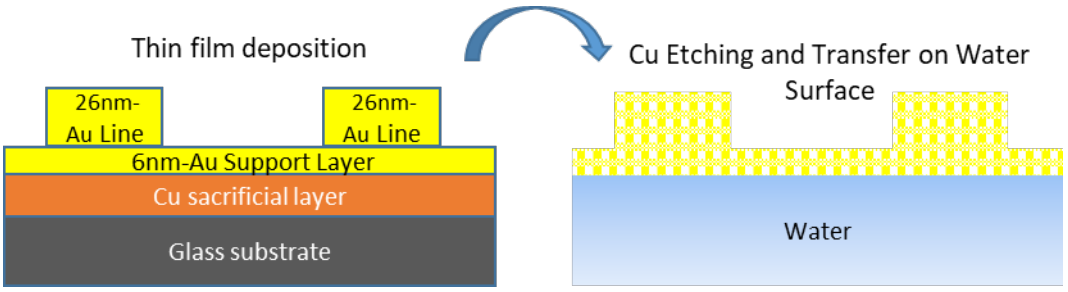

Figure 7. Schematic representation of the layers, including the Au support layer and the patterns to be transferred.

Figure 8. Transfer of a horseshoe design on a 3D surface. The width of the lines is 3 mm.

CONCLUSION

Freestanding ultra-thin nanoporous gold films can be obtained on the surface of water and transferred to the surface of PET with surface areas of up to around 100 cm^2. There is nothing in this process to prevent scaling up to larger surfaces, beyond 100 cm^2. The minimum critical thickness of gold layers is between 6 nm and 13 nm. Films that are too thin suffer from fragmentation after copper etching, resulting in a loss of electrical conductivity due to cracks. From a thickness of 13 nm, the transfer can take place without any crack formation and film fragmentation. These thicker films have properties in terms of sheet resistance and transmittance ranging from a few Ω/□ for 56 nm-thick films, not transparent, to about tens Ω/□ for 13 nm-thick films with a transparency of the order of 50 %. Transferred films, whatever their equivalent Au thickness (13, 26, or 56 nm) can withstand flexion cycles up to a curvature radius of 1 mm on PET substrate corresponding to a tensile strain of 6.5 %. It is worth noticing that, in comparison, films of equivalent thickness directly deposited on PET do not withstand the flexion test and lose their conductivity. The excellent flexibility performance of the transferred films could be attributed to the specific 2D morphology consisting of a nanoporous microstructure induced by Cu etching process. This remarkable change in behavior between the direct deposited films and the transferred layers must be emphasized and will be the subject of future work.

We also observe differences between transferred pure Au films and transferred dealloyed films: for a given equivalent Au thickness, dealloyed films present the highest sheet resistance and lowest mechanical behavior under tensile strain, which could be attributed to the difference of morphology and microstructural defects introduced by the dealloying process.

Transferring patterns from such ultrathin layers onto surfaces of 3D objects is possible using an additional support 6 nm thick layer that holds the pattern during the transfer operation. This kind of process could lead to potential applications in flexible electronics where an Au semitransparent flexible patterned electrode would be required on the surface of complex 3D

shapes. Transferring such a flat patterned layer on a 3D object has proved very easy, provided a very thin support layer was used.

Acknowledgment

The authors acknowledge F. Petitgas (IMN Nantes) and Florian Massuyeau (IMN Nantes) for their technical assistance on the co-sputtering system and the optical absorption measurements respectively. The authors also gratefully acknowledge N. Stephant (Nantes University) and Cédric Doutriaux (Nantes University) for their technical support on the SEM images of the nanoporous films and the development of flexible tests respectively. The authors thank the NanoRennes platform belonging to RENATECH+ (the French national network of facilities for micronanotechnology).

Supporting information.

Film deposition and EDS, XPS, Optical transmittance, 3D surface design, Horseshoe pattern, SEM image.

References

(1) Lee, S.; Shi, Q.; Lee, C. From Flexible Electronics Technology in the Era of IoT and Artificial Intelligence toward Future Implanted Body Sensor Networks. *APL Mater.* **2019**, *7* (3), 031302. https://doi.org/10.1063/1.5063498.

(2) Yogeswaran, N.; Dang, W.; Navaraj, W. T.; Shakthivel, D.; Khan, S.; Polat, E. O.; Gupta, S.; Heidari, H.; Kaboli, M.; Lorenzelli, L.; Cheng, G.; Dahiya, R. New Materials and Advances in Making Electronic Skin for Interactive Robots. *Adv. Robot.* **2015**, *29* (21), 1359–1373. https://doi.org/10.1080/01691864.2015.1095653.

(3) Yang, T.; Xie, D.; Li, Z.; Zhu, H. Recent Advances in Wearable Tactile Sensors: Materials, Sensing Mechanisms, and Device Performance. *Mater. Sci. Eng. R Rep.* **2017**, *115* (Supplement C), 1–37. https://doi.org/10.1016/j.mser.2017.02.001.

(4) Stoppa, M.; Chiolerio, A. Wearable Electronics and Smart Textiles: A Critical Review. *Sensors* **2014**, *14* (7), 11957–11992. https://doi.org/10.3390/s140711957.

(5) Stadlober, B.; Zirkl, M.; Irimia-Vladu, M. Route towards Sustainable Smart Sensors: Ferroelectric Polyvinylidene Fluoride-Based Materials and Their Integration in Flexible

Electronics. *Chem. Soc. Rev.* **2019**, *48* (6), 1787–1825. https://doi.org/10.1039/C8CS00928G.

(6) Shintake, J.; Cacucciolo, V.; Floreano, D.; Shea, H. Soft Robotic Grippers. *Adv. Mater.* **2018**, *30* (29), 1707035. https://doi.org/10.1002/adma.201707035.

(7) Shi, J.; Liu, S.; Zhang, L.; Yang, B.; Shu, L.; Yang, Y.; Ren, M.; Wang, Y.; Chen, J.; Chen, W.; Chai, Y.; Tao, X. Smart Textile-Integrated Microelectronic Systems for Wearable Applications. *Adv. Mater.* **2020**, *32* (5), 1901958. https://doi.org/10.1002/adma.201901958.

(8) Cui, N.; Song, Y.; Tan, C.-H.; Zhang, K.; Yang, X.; Dong, S.; Xie, B.; Huang, F. Stretchable Transparent Electrodes for Conformable Wearable Organic Photovoltaic Devices. *Npj Flex. Electron.* **2021**, *5* (1), 1–8. https://doi.org/10.1038/s41528-021-00127-7.

(9) Cheng, T.; Zhang, Y.; Lai, W.-Y.; Huang, W. Stretchable Thin-Film Electrodes for Flexible Electronics with High Deformability and Stretchability. *Adv. Mater.* **2015**, *27* (22), 3349–3376. https://doi.org/10.1002/adma.201405864.

(10) Pang, C.; Lee, C.; Suh, K.-Y. Recent Advances in Flexible Sensors for Wearable and Implantable Devices: Review. *J. Appl. Polym. Sci.* **2013**, *130* (3), 1429–1441. https://doi.org/10.1002/app.39461.

(11) Zhu, Y.; Li, J.; Kim, J.; Li, S.; Zhao, Y.; Bahari, J.; Eliahoo, P.; Li, G.; Kawakita, S.; Haghniaz, R.; Gao, X.; Falcone, N.; Ermis, M.; Kang, H.; Liu, H.; Kim, H.; Tabish, T.; Yu, H.; Li, B.; Akbari, M.; Emaminejad, S.; Khademhosseini, A. Skin-Interfaced Electronics: A Promising and Intelligent Paradigm for Personalized Healthcare. *Biomaterials* **2023**, *296*, 122075. https://doi.org/10.1016/j.biomaterials.2023.122075.

(12) Wang, Y.; Hong, T.; Wang, L.; Li, G.; Bai, N.; Li, C.; Lu, P.; Cai, M.; Wu, Z.; Lu, N.; Yu, B.; Zhang, J.; Guo, C. F. Epidermal Electrodes with Enhanced Breathability and High Sensing Performance. *Mater. Today Phys.* **2020**, *12*, 100191. https://doi.org/10.1016/j.mtphys.2020.100191.

(13) Nguyen, V. H.; Papanastasiou, D. T.; Resende, J.; Bardet, L.; Sannicolo, T.; Jiménez, C.; Muñoz-Rojas, D.; Nguyen, N. D.; Bellet, D. Advances in Flexible Metallic Transparent Electrodes. *Small* **2022**, *18* (19), 2106006. https://doi.org/10.1002/smll.202106006.

(14) Li, W.; Meredov, A.; Shamim, A. Coat-and-Print Patterning of Silver Nanowires for Flexible and Transparent Electronics. *Npj Flex. Electron.* **2019**, *3* (1), 1–7. https://doi.org/10.1038/s41528-019-0063-3.

(15) Lu, X.; Zhang, Y.; Zheng, Z. Metal-Based Flexible Transparent Electrodes: Challenges and Recent Advances. *Adv. Electron. Mater. n/a* (n/a), 2001121. https://doi.org/10.1002/aelm.202001121.

(16) Feng, Y.; Song, J.; Han, G.; Zhou, B.; Liu, C.; Shen, C. Transparent and Stretchable Electromagnetic Interference Shielding Film with Fence-like Aligned Silver Nanowire Conductive Network. *Small Methods n/a* (n/a), 2201490. https://doi.org/10.1002/smtd.202201490.

(17) Harris, K. D.; Elias, A. L.; Chung, H.-J. Flexible Electronics under Strain: A Review of Mechanical Characterization and Durability Enhancement Strategies. *J. Mater. Sci.* **2016**, *51* (6), 2771–2805. https://doi.org/10.1007/s10853-015-9643-3.

(18) Akogwu, O.; Kwabi, D.; Munhutu, A.; Tong, T.; Soboyejo, W. O. Adhesion and Cyclic Stretching of Au Thin Film on Poly(Dimethyl-Siloxane) for Stretchable Electronics. *J. Appl. Phys.* **2010**, *108* (12), 123509. https://doi.org/10.1063/1.3510488.

(19) De, S.; Higgins, T. M.; Lyons, P. E.; Doherty, E. M.; Nirmalraj, P. N.; Blau, W. J.; Boland, J. J.; Coleman, J. N. Silver Nanowire Networks as Flexible, Transparent, Conducting Films: Extremely High DC to Optical Conductivity Ratios. *ACS Nano* **2009**, *3* (7), 1767–1774. https://doi.org/10.1021/nn900348c.

(20) Park, S.-M.; Jang, N.-S.; Ha, S.-H.; Kim, K. H.; Jeong, D.-W.; Kim, J.; Lee, J.; Kim, S. H.; Kim, J.-M. Metal Nanowire Percolation Micro-Grids Embedded in Elastomers for Stretchable and Transparent Conductors. *J. Mater. Chem. C* **2015**, *3* (31), 8241–8247. https://doi.org/10.1039/C5TC00740B.

(21) Guo, C. F.; Ren, Z. Flexible Transparent Conductors Based on Metal Nanowire Networks. *Mater. Today* **2015**, *18* (3), 143–154. https://doi.org/10.1016/j.mattod.2014.08.018.

(22) Cheng, T.; Zhang, Y.-Z.; Lai, W.-Y.; Chen, Y.; Zeng, W.-J.; Huang, W. High-Performance Stretchable Transparent Electrodes Based on Silver Nanowires Synthesized via an Eco-Friendly Halogen-Free Method. *J Mater Chem C* **2014**, *2* (48), 10369–10376. https://doi.org/10.1039/C4TC01959H.

(23) Benetti, G.; Banfi, F.; Cavaliere, E.; Gavioli, L. Mechanical Properties of Nanoporous Metallic Ultrathin Films: A Paradigmatic Case. *Nanomaterials* **2021**, *11* (11), 3116. https://doi.org/10.3390/nano11113116.

(24) Kwon, H.; Barad, H.-N.; Silva Olaya, A. R.; Alarcón-Correa, M.; Hahn, K.; Richter, G.; Wittstock, G.; Fischer, P. Dry Synthesis of Pure and Ultrathin Nanoporous Metallic Films. *ACS Appl. Mater. Interfaces* **2023**. https://doi.org/10.1021/acsami.2c19584.

(25) Zhu, J.; Han, D.; Wu, X.; Ting, J.; Du, S.; Arias, A. C. Highly Flexible Transparent Micromesh Electrodes via Blade-Coated Polymer Networks for Organic Light-Emitting Diodes. *ACS Appl. Mater. Interfaces* **2020**, *12* (28), 31687–31695. https://doi.org/10.1021/acsami.0c07299.

(26) Guo, C. F.; Sun, T.; Liu, Q.; Suo, Z.; Ren, Z. Highly Stretchable and Transparent Nanomesh Electrodes Made by Grain Boundary Lithography. *Nat. Commun.* **2014**, *5* (1). https://doi.org/10.1038/ncomms4121.

(27) Li, L.; Zhang, B.; Zou, B.; Xie, R.; Zhang, T.; Li, S.; Zheng, B.; Wu, J.; Weng, J.; Zhang, W.; Huang, W.; Huo, F. Fabrication of Flexible Transparent Electrode with Enhanced Conductivity from Hierarchical Metal Grids. *ACS Appl. Mater. Interfaces* **2017**, *9* (45), 39110–39115. https://doi.org/10.1021/acsami.7b12298.

(28) Harnois, M.; Himdi, M.; Yong, W. Y.; Rahim, S. K. A.; Tekkouk, K.; Cheval, N. An Improved Fabrication Technique for the 3-D Frequency Selective Surface Based on Water

Transfer Printing Technology. *Sci. Rep.* **2020**, *10* (1), 1714. https://doi.org/10.1038/s41598-020-58657-5.

(29) Le Borgne, B.; De Sagazan, O.; Crand, S.; Jacques, E.; Harnois, M. Conformal Electronics Wrapped Around Daily Life Objects Using an Original Method: Water Transfer Printing. *ACS Appl. Mater. Interfaces* **2017**, *9* (35), 29424–29429. https://doi.org/10.1021/acsami.7b07327.

(30) Chauvin, A.; Heu, W. T. C.; Buh, J.; Tessier, P.-Y.; Mel, A.-A. E. 2019 - Vapor Dealloying of Ultra-Thin Films: A Promising Concept for the Fabrication of Highly Flexible Transparent Conductive Metal Nanomesh Electrodes. *Npj Flex. Electron.* **2019**, *3* (1), 5. https://doi.org/10.1038/s41528-019-0049-1.

(31) Le Borgne, B.; Jacques, E.; Harnois, M. The Use of a Water Soluble Flexible Substrate to Embed Electronics in Additively Manufactured Objects: From Tattoo to Water Transfer Printed Electronics. *Micromachines* **2018**, *9* (9), 474. https://doi.org/10.3390/mi9090474.

(32) Ding, Y.; Kim, Y.-J.; Erlebacher, J. Nanoporous Gold Leaf: ?Ancient Technology?/Advanced Material. *Adv. Mater.* **2004**, *16* (21), 1897–1900. https://doi.org/10.1002/adma.200400792.

(33) Zhang, Z.; Wang, Y.; Qi, Z.; Zhang, W.; Qin, J.; Frenzel, J. Generalized Fabrication of Nanoporous Metals (Au, Pd, Pt, Ag, and Cu) through Chemical Dealloying. *J. Phys. Chem. C* **2009**, *113* (29), 12629–12636. https://doi.org/10.1021/jp811445a.

(34) Erlebacher, J.; Aziz, M. J.; Karma, A.; Dimitrov, N.; Sieradzki, K. Evolution of Nanoporosity in Dealloying. *Nature* **2001**, *410* (6827), 450–453. https://doi.org/10.1038/35068529.

(35) Niauzorau, S.; Sharstniou, A.; Sampath, V. K.; Kublik, N.; Bandarenka, H.; Azeredo, B. Electroless Dealloying of Thin-Film Nanocrystalline Au–Ag Alloys: Mechanisms of Ligament Nucleation and Sources of Its Synthesis Variability. *ACS Appl. Mater. Interfaces* **2022**, *14* (15), 17927–17939. https://doi.org/10.1021/acsami.1c24388.

(36) *Nanoporous Gold: From an Ancient Technology to a High-Tech Material*; Wittstock, A., Biener, J., Erlebacher, J., Bäumer, M., Eds.; Nanoscience & Nanotechnology Series; Royal Society of Chemistry: Cambridge, 2012. https://doi.org/10.1039/9781849735285.

(37) Chauvin, A.; Lafuente, M.; Mevellec, J. Y.; Mallada, R.; Humbert, B.; Pina, M. P.; Tessier, P.-Y.; Mel, A. E. Lamellar Nanoporous Gold Thin Films with Tunable Porosity for Ultrasensitive SERS Detection in Liquid and Gas Phase. *Nanoscale* **2020**. https://doi.org/10.1039/D0NR01721C.

(38) Shahine, I.; Mevellec, J.-Y.; Richard-Plouet, M.; Humbert, B.; Tessier, P.-Y. Nanoporous Gold Stacked Layers as Substrates for SERS Detection in Liquids or Gases with Ultralow Detection Limits and Long-Term Stability. *J. Phys. Chem. C* **2022**, acs.jpcc.2c05903. https://doi.org/10.1021/acs.jpcc.2c05903.

(39) Wang, T.; Park, M.; Yu, Q.; Zhang, J.; Yang, Y. Stability and Synthesis of 2D Metals and Alloys: A Review. *Mater. Today Adv.* **2020**, *8*, 100092. https://doi.org/10.1016/j.mtadv.2020.100092.

(40) Balbaud, F.; Sanchez, G.; Santarini, G.; Picard, G. Equilibria Between Gas and Liquid Phases for Concentrated Aqueous Solutions of Nitric Acid. *Eur. J. Inorg. Chem.* **1999**, *1999* (2), 277–285. https://doi.org/10.1002/(SICI)1099-0682(19990202)1999:2<277::AID-EJIC277>3.0.CO;2-#.

(41) Chauvin, A.; Txia Cha Heu, W.; Buh, J.; Tessier, P.-Y.; El Mel, A.-A. Vapor Dealloying of Ultra-Thin Films: A Promising Concept for the Fabrication of Highly Flexible Transparent Conductive Metal Nanomesh Electrodes. *Npj Flex. Electron.* **2019**, *3* (1), 5. https://doi.org/10.1038/s41528-019-0049-1.

(42) Le Borgne, B.; De Sagazan, O.; Crand, S.; Jacques, E.; Harnois, M. Conformal Electronics Wrapped Around Daily Life Objects Using an Original Method: Water Transfer Printing. *ACS Appl. Mater. Interfaces* **2017**, *9* (35), 29424–29429. https://doi.org/10.1021/acsami.7b07327.

(43) Harnois, M.; Garcia-Castro, F.; Herry, G.; De Sagazan, O.; Le Bihan, F. Eco-Designed Conformable Inorganic Electronics to Improve the End of Life of Smart Objects: Sensor Processing and Applications. *ACS Appl. Electron. Mater.* **2020**, *2* (2), 563–570. https://doi.org/10.1021/acsaelm.9b00807.

(44) Wittstock, G.; Bäumer, M.; Dononelli, W.; Klüner, T.; Lührs, L.; Mahr, C.; Moskaleva, L. V.; Oezaslan, M.; Risse, T.; Rosenauer, A.; Staubitz, A.; Weissmüller, J.; Wittstock, A. Nanoporous Gold: From Structure Evolution to Functional Properties in Catalysis and Electrochemistry. *Chem. Rev.* **2023**, *123* (10), 6716–6792. https://doi.org/10.1021/acs.chemrev.2c00751.

(45) Zhang, Y.; Luo, F.; Bai, Q.; Zhang, C.; Yu, B.; Zhang, Z. In-Situ X-Ray Diffraction Study on Dealloying: A Scenario of a Cu90Au10 Alloy. *J. Phys. Chem. Solids* **2021**, *150*, 109879. https://doi.org/10.1016/j.jpcs.2020.109879.

For Table of Contents Use Only